Volume 1 | Number 1 | Jan 2013 | Pages 1–100

Nanoscale

www.rsc.org/nanoscale

ROYAL SOCIETY OF CHEMISTRY

ROYAL SOCIETY OF CHEMISTRY

www.rsc.org/nanoscale

ARTICLE TYPE

Nano-grid structure made of perovskite SrTiO₃ nanowires for efficient electron transport layers in inverted polymer solar cells

Jeong Won Kim[a], Yo-han Suh[a], Chang-Lyoul Lee[b], Yong Seok Kim[c], and Won Bae Kim[a,d]*

A nano-grid structure of perovskite SrTiO₃ NWs is developed for novel electron transport layer in inverted polymer solar cells. Due to the excellent charge transporting properties of SrTiO₃ nano-grid structure, the device employing this
10 **nanostructure showed ~32 % enhanced photovoltaic performance, compared to the solar cell using TiO₂ thin film.**

The bulk-heterojunction (BHJ) polymer solar cells (PSCs) consisting of conjugated polymers (photo-active polymer, electron donor) and fullerene derivatives (electron acceptor) have
15 received lots of attention as next generation energy conversion system due to their outstanding advantages such as light weight, low cost and simple fabrication in large area.[1, 2] However, the BHJ-PSCs still need improvement in terms of power conversion efficiency (PCE) and long-term air stability for
20 commercialization.[3-6] To overcome these issues, the inverted PSCs have been proposed and developed through the modification and optimization of the device structure.[7, 8]

As an electron transport layer (ETL) in the inverted PSCs, *n*-type metal oxides have many beneficial properties such as
25 environmental stability, high transparency, remarkable electron transport and hole blocking property. Among the several kinds of *n*-type metal oxides, especially, TiOₓ and ZnO have been widely used as an ETL in inverted PSCs.[9-13] However, the relative energy level mismatch (~0.5eV) between the conduction band energy of
30 *n*-type metal oxides and the lowest unoccupied molecular orbital (LUMO) level of fullerene derivatives is one of drawbacks to be solved in order to improve device performance in the inverted PSCs. To reduce the difference between the energy levels, the *n*-type doping method such as nitrogen[14, 15] or zirconium[16, 17]
35 doping into TiO₂ is widely used to alter the conduction band energy level. Unfortunately, there is still a weakness caused from a commercial viewpoint due to the difficulty in controlling the exact doping concentration as well as price issue of doping material and processing. Therefore, it is strongly required for the
40 development and synthesis of new materials, of which the conduction band is located closer to the vacuum level without losing other excellent properties of *n*-type metal oxides.

1-dimensional (1-D) nanostructures such as nanowires (NWs), nanorods, and nanoneedles have attracted a lot of
45 attention in nanoscale opto-electronic devices due to their unique, controllable and multi-functional properties.[18-20] Especially, metal oxide having 1-D nanostructures can show excellent properties as an electrode in opto-electronic devices because they could diminish the charge recombination in the photo-active layer
50 through rapid charge transfer along their direct pathway and efficient carrier percolation at the interface.[21-24] In this respect, the utilization of *n*-type metal oxides with 1-D nanostructures as an ETL can be very practical and ideal solutions for realizing highly efficient inverted PSCs.[25, 26]

55 In this study, the inverted PSCs which employ strontium titanate (SrTiO₃) NWs as an ETL were newly introduced and their photovoltaic performances were investigated. SrTiO₃ is a cubic structured perovskite crystal which has the ABO₃ stoichiometry, but its crystal structure is very similar to that of
60 anatase TiO₂. Also, the band-gap energies of both perovskite SrTiO₃ and anatase TiO₂ are almost same (approximately 3.2 eV). However, the conduction band of SrTiO₃ is located closer to the vacuum level than that of TiO₂ by 0.2 eV. This negative shift of conduction band in SrTiO₃ can significantly reduce charge
65 recombination in the photo-active layer with efficient charge extraction from the LUMO level of fullerene derivatives to the conduction band of SrTiO₃.[27, 28] In addition to efficient charge extraction from photo-active layer, nano-grid structures of metal oxide NWs in the inverted PSCs offer efficient percolating
70 pathways and large contact area by building an interpenetrated network structure between photo-active layer and cathode electrode. The nano-grid structures of TiO₂ NWs and SrTiO₃ NWs used in this work were synthesized on the cathode electrode *via* a facile electrospinning method. The inverted PSCs
75 employing the SrTiO₃ nano-grid structure as an ETL exhibited significant improvement of power conversion efficiency by 32 %, compared to that of the reference cell with TiO₂ thin film (TF) as the ETL.

Electrospinning solution for TiO₂ NWs was prepared by
80 chemical synthetic processes. Firstly, 0.375 ml of titanium butoxide was mixed with solution of acetic acid (0.75 ml) and ethanol (0.75 ml) under stirring in N₂ atmosphere. The mixed solution was then blended with 0.112 g of polyvinyl pyrrolidone (PVP) dissolved in 1.875 ml of ethanol. The electrospinning
85 precursor solution for SrTiO₃ NWs was also prepared similarly. Firstly, 0.113 g of strontium acetate and 0.188 ml of titanium butoxide were mixed in the solution consisting of 1.5 ml of acetic acid and 1 ml of ethanol under constant stirring at 60 °C in N₂-filled glove box. Herein, the nominal molar ratio of Sr:Ti was
90 controlled to 1:1. After enough stirring at 60 °C, the precursor solutions were blended with the PVP solution which was homogenously prepared by dissolving 0.108 g of PVP in 1 ml of ethanol. Each mixture solution of TiO₂ and SrTiO₃ was separately loaded into a plastic syringe equipped with a cutted 23 gauge
95 (inner diameter of ca. 0.42 μm) needle made of stainless steel. The needle was connected to a high- voltage supply (DC high voltage generator, CPS-40K03VIT). The indium tin oxide (ITO)

(Nanoscale Accepted Manuscript)
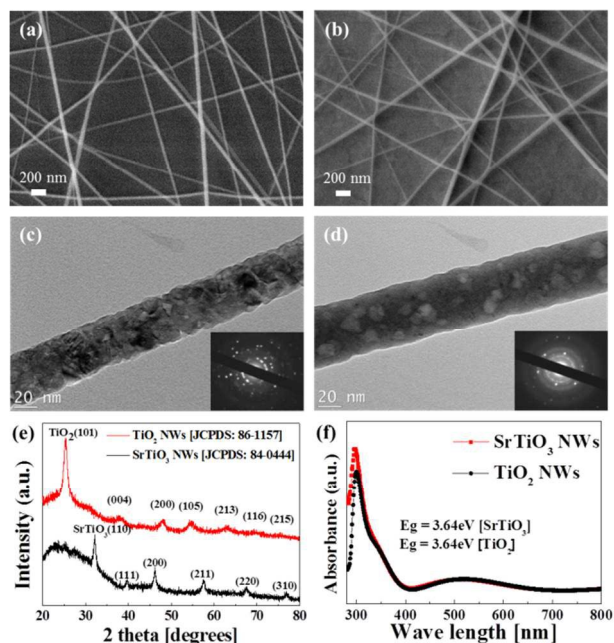
Fig. 1 FE-SEM images of (a) electrospun TiO₂ NWs and (b) electrospun SrTiO₃ NWs on ITO substrate. HR-TEM images (inset images: selected area diffraction pattern) of (c) electrospun TiO₂ and (d) SrTiO₃ NW. (e) XRD patterns and (f) UV-Visible spectra of TiO₂ and SrTiO₃ NWs.

glass substrate coated with metal oxides TF (~10 nm) *via* sol-gel process was loaded on a metallic collector. When applying a high voltage between the syringe needle and the substrate, the electrospun NWs were collected on the substrate. Finally, as-electrospun NWs on the substrates were calcined in a furnace at 500 °C for 3 h in air.

From the FE-SEM images in Fig. 1 (a) and (b), it was observed that the synthesized TiO₂ NWs and SrTiO₃ NWs have ultra-long length (> 5 μm) with diameters in range of 30~70 nm. The nano-grid structures of TiO₂ NWs and SrTiO₃ NWs were formed on the substrates with the control of NWs density by changing electrospinning condition. The TEM images in Fig. 1(c) and (d) represent local structural properties of an individual NW of TiO₂ and SrTiO₃, respectively. The selected area electron diffraction (SAED) patterns showed the diffuse ring patterns with clear spots, indicating both TiO₂ NWs and SrTiO₃ NWs are polycrystalline structure (Insets of Fig. 1(c) and (d)). XRD results in Fig. 1(e) revealed that the electrospun TiO₂ NWs and SrTiO₃

NWs are consisted of anatase TiO₂ phase (titanate, JCPDS card No. 86-1157) and cubic- perovskite SrTiO₃ phase (strontium titanate, JCPDS card No. 84-0444), respectively. In order to identify composition elements and relative proportions in both TiO₂ NWs and SrTiO₃ NWs, the atomic elemental analysis was performed by EDX as shown in Fig. S1. From the EDX spectra, it is confirmed that the electrospun TiO₂ NWs and SrTiO₃ NWs are mainly consisted of Sr, Ti, and O elements. The UV/Vis absorption spectra were measured to study the optical properties of the electrospun NWs. As described above, the absorption patterns of the synthesized TiO₂ NWs and SrTiO₃ NWs are almost same with similar bandgap of 3.64 eV at the visible light range as shown in Fig. 1(f).

Fig. 2(a) describes the schematic illustration of the inverted PSCs which use the ETL consisting of metal oxide (TiO₂ or SrTiO₃) NWs as the electron extractor and the pathway for electron transport. Firstly, thin and planar film layers of TiO₂ or SrTiO₃ (ca. 10 nm) were uniformly deposited *via* a sol-gel process on the ITO substrate in order to prevent hole transport. Next, the nano-grid structures of TiO₂ NWs or SrTiO₃ NWs were fabricated as an ETL over the thin film layer by electrospinning processes. The poly[3-hexylthiophene](P3HT):*phenyl-C₆₁-butyric acid methyl ester* (PCBM) layer was spin-coated on the ETL and applied in inverted PSCs as the photo-active layer. Covering nano-grid architecture of NWs with conjugated polymer film can provide three-dimensional inorganic-organic connection (i.e., interpenetrating structure) by infiltrating the blend (P3HT:PCBM) into the nano-grid structure (See Fig. S2 of the ESI).[29-31] This interpenetrating structure increases contact area between the ETL and photo-active layer, compared to simple planar structure. In this inverted PSC structure, the photo-generated charge carriers (holes and electrons) are transported along the percolating pathways to the relevant electrodes as shown in Fig. 2a, in which electron and hole move toward the cathode (ITO) *via* the NWs and the anode (Ag/MoO₃), respectively. Fig. 2(b) depicts the corresponding energy levels of the materials used in this inverted PSCs. In the energy level diagram of Fig. 2(b), SrTiO₃ has a higher conduction band position, compared to TiO₂. This can result in efficient electron transporting from LUMO of PCBM to conduction band of SrTiO₃.

To investigate photovoltaic performance with the different ETL structures such as TiO₂ TF, TiO₂ TF/NWs and SrTiO₃ TF/NWs (See Fig. S3 of the ESI), inverted PSCs consisting of ITO/*n*-type metal oxides/P3HT:PCBM/MoO₃/Ag were fabricated. The photovoltaic performances of the inverted PSCs were investigated by measuring the current–voltage (*J-V*) and IPCE
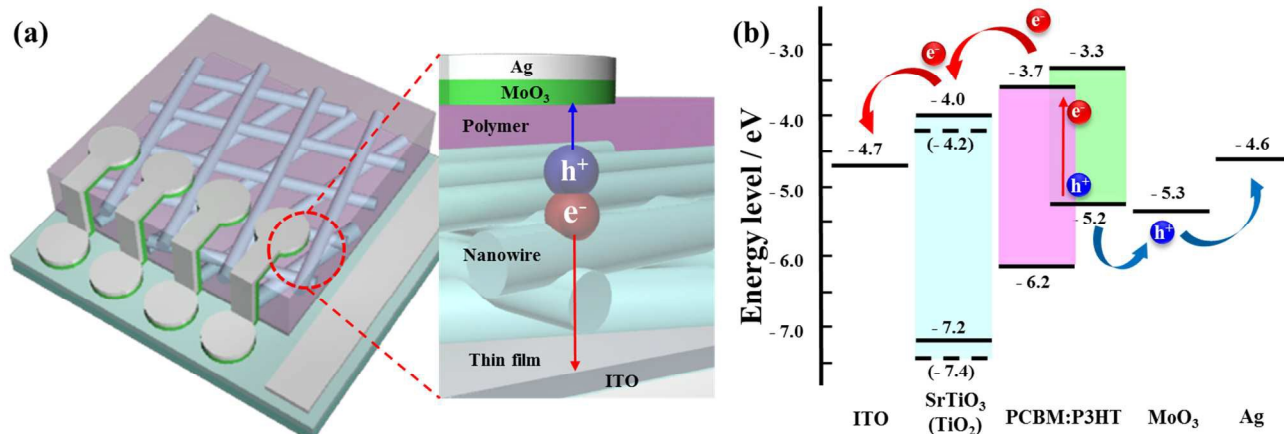
Fig. 2 (a) A schematic illustration of the inverted PSCs with electrospun nano-grid structure as the electron acceptor. (b) The energy level diagrams of the materials used in the inverted PSCs.

(Fig. 3(a) and (b)). Table 1 summarized the photovoltaic
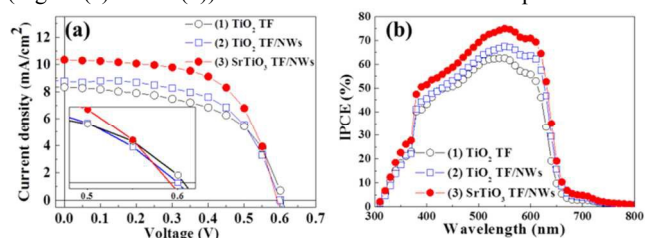
Fig. 3 (a) *I-V* characteristics and (b) IPCE curves of inverted PSCs employing different ETLs.

performances of inverted PSCs with the different ETLs. Also, Fig. S4 presents the statistical analysis of the photovoltaic parameters. The photocurrent (J_{sc}) obtained from current–voltage
5 (J-V) was calibrated from the IPCE to ensure the accuracy of the measurement. The 1-D nanostructures in photovoltaic devices can induce the better charge transport from photo-active layer into electrode because the 1-D nanostructures such as NWs can provide direct pathway along their longitudinal morphologies at
10 the interfacial connection.[32] By taking advantage of the efficient charge transport of NWs, inverted PSC (device 2) employing the nano-grid structure of TiO$_2$ NWs as the ETL showed the better photovoltaic performance by an increase of photocurrent (J_{sc}) and Fill factor (FF) than that of inverted PSC (device 1) using TiO$_2$
15 TF, as shown in Fig. 3(a) and Table 1. Moreover, it is noticeable that photovoltaic performance of the inverted PSC (device 3) employing nano-grid structure of SrTiO$_3$ NWs as the ETL exhibited significant enhancement (~20%) in the photovoltaic performance, compared with the inverted PSC (device 2)
20 employing nano-grid structure of TiO$_2$ NWs (Fig. 3(a) and Table 1). It is expected that the main reason for the enhancement of photovoltaic performance in the device 3 is improved electron transporting properties due to higher electron affinity of SrTiO$_3$, which could be induced from better energy level match between
25 the PCBM and metal oxide. Consequently, the device 3 showed ~32 % enhancement in PCE with improving photocurrent (J_{sc}) and FF compared to that of reference device (device 1).

   Generally, photovoltaic performance, especially photocurrent (J_{sc}), is directly related with the charge carrier density induced by
30 light absorption in photo-active layer.[33] Therefore, transmittance spectra of the different ETLs and light absorbance spectra of each photo-active layer (P3HT:PCBM), coated on the ETLs, were measured by UV-vis absorption spectroscopy to investigate that enhancement of photovoltaic performance might be originated
35 from improvement of the photo-induced charge carrier density (See Fig. S5 of the ESI). As shown in the Fig. S5(a), the transmittance shapes of the three ETLs are almost same. However, the transmittance intensities of the nano-grid structures made of metal oxides NWs are relatively lower than that of the
40 TF structure in the range of 400 to 500 nm. This is an opposite trend against the photovoltaic performances shown in Fig. 3(a)
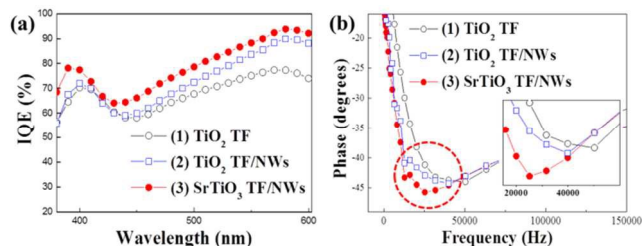
Fig. 4 (a) Internal quantum efficiency (IQE) of inverted PSCs employing the different ETLs. (b) Bode plot for EIS measurement obtained from inverted PSCs employing different ETLs under one-sun illumination.

Table 1. Photovoltaic performance of inverted PSCs with the different ETLs [a].

Electron transport layer components	V$_{oc}$ [V]	J$_{sc}$ [mA/cm^2]	Fill factor [%]	Efficiency [%]	Carrier lifetime [μs]
(1) TiO$_2$ TF	0.61	8.3	55.9	2.8	3.2
(2) TiO$_2$ TF / NWs	0.60	8.8	58.7	3.1	4.0
(3) SrTiO$_3$ TF / NWs	0.59	10.4	61.0	3.7	6.3

[a] Radiant power: 100 mW/cm^2 (AM 1.5 G), Cell area: 4.75 x 10^{-6} cm^2

45 and Table 1. For instance, the device 1 with TiO$_2$ TF as ETL showed the lower photocurrent (J_{sc}) than those of devices 2 and 3 with nano-grid structures of TiO$_2$ NWs and SrTiO$_3$ NWs in spite of higher light absorption in photo-active layer as shown in Fig. S5(b) of the ESI. In addition, the device 3 using nano-grid
50 structure of SrTiO$_3$ NWs as ETL shows much higher photovoltaic performance than that of device 2 with nano-grid structure of TiO$_2$ NWs, even though light absorption of the photo-active layer in devices 2 and 3 is similar as shown in Fig. S5(b). The internal quantum efficiency (IQE) spectra in Fig. 4(a) show the efficiency
55 of collected carriers per absorbed photon.[34] As shown in Fig. 4(a), the inverted PSCs (device 3) employing SrTiO$_3$ nano-grid structure have the highest IQE value. This result strongly suggested that higher photovoltaic performance of device 3 is attributed to the excellent charge extraction and transporting
60 properties of SrTiO$_3$ nano-grid structure as the ETL.

   The charge transporting properties of the different ETLs in the inverted PSCs were measured and analyzed using electrical impedance spectroscopy (EIS). Fig. 4(b) shows Bode plots of EIS in the inverted PSCs with the different ETLs. As shown in the
65 Fig. 4(b), the characteristic peak, frequency value at the lowest phase angle, was shifted to lower frequency range in the order of device 3, device 2 and device 1. Herein, the frequency value of the characteristic peak in Bode plots determined the electron lifetime (τ_e) in the inverted PSCs using the following equation:
70

$$\tau_e = \frac{1}{2\pi f_{characteristic}}$$

where $f_{characteristic}$ is the value of characteristic frequency at the lowest phase angle.[35] The calculated τ_e values were summarized in Table 1. Interestingly, the electron lifetimes at the
75 ETLs/polymer interfaces are similarly increasing in correspondence with the improvement of photovoltaic performance in the inverted PSCs with the different ETLs (See Table 1). Especially, the device 3 employing the SrTiO$_3$ nano-grid ETL shows two times longer carrier lifetime than that of the
80 device 1 employing TiO$_2$ TF ETL. The longer carrier lifetime at the interface indicates the reduction of charge recombination and low resistance at the interface by efficient charge transporting from the photo-active layer to an ETL.[36] From the inset of Fig. 3a, the series resistance (R$_s$) of inverted PSCs with different ETLs
85 was obtained by the slopes of *J-V* curve at V$_{oc}$ (near 0.6 V). R$_s$ is determined by the inverse value of the slope at V$_{oc}$. As expected, the device 3 with the SrTiO$_3$ nano-grid structure showed the lowest R$_s$, compared to that of the devices 1 and 2 made of TiO$_2$ TF and nano-grid structure, respectively. These results imply the
90 beneficial role of SrTiO$_3$ nano-grid structure on charge extraction and transfer from high conduction band and effective electron pathway at the interface between the ETL and photo-active layer in the inverted PSCs. Therefore, inverted PSCs employing the nano-grid structures of SrTiO$_3$ NWs as an ETL exhibited the
95 significant improvement of PCE by enhanced current density and FF, even though the nano-grid structure showed a relatively poor

transmittance under the visible light range.

Conclusions

We introduced the nano-grid structure of $SrTiO_3$ NWs in inverted PSCs as an ETL to improve the electron extraction and transfer at the interface between inorganic nanostructures and photo-active polymer. The nano-grid structure of $SrTiO_3$ NWs was easily synthesized by electrospinning method on the cathode electrode. The higher conduction band of $SrTiO_3$ significantly reduced charge recombination of the carriers created in the photo-active layer due to efficient charge extraction from LUMO level of fullerene derivatives, compared to the TiO_2 materials. Moreover, the nano-grid structure of $SrTiO_3$ NWs showed enhanced electron transporting properties by efficient percolating pathways and large contact area by building an interpenetrated network structure between photo-active layer and cathode electrode. As a result, the inverted PSCs employing the $SrTiO_3$ nano-grid structures as an effective ETL showed the enhanced photovoltaic performance by ca. 32 %, compared to that of inverted PSCs with TiO_2 TF. The novel $SrTiO_3$ ETL system in this study would provide a promising approach to improve carrier transport properties on the various opto-electronic devices.

Acknowledgements

Notes and references

a School of Materials Science and Engineering, Gwangju Institute of Science and Technology (GIST), 261 Cheomdan-gwagiro, Buk-gu, Gwangju 500-712, Republic of Korea.

b Advanced Photonics Research Institute (APRI), Gwangju Institute of Science and Technology (GIST), Gwangju, Republic of Korea

c School of Chemical and Biomolecular Engineering, Cornell University, 120 Olin Hall, Ithaca, New York 14853-5201, USA.

d Research Institute for Solar and Sustainable Energies (RISE), Gwangju Institute of Science and Technology (GIST), Republic of Korea

† Electronic supplementary information (ESI) available: [Experimental detail, HR-TEM images with EDX atomic ratio analysis, FE-SEM images, transmittance spectra and light absorbance spectra]. See DOI: 10.1039/c000000x/

1. N. S. Sariciftci, L. Smilowitz, A. J. Heeger and F. Wudi, *Science*, 1992, **258**, 1474.
2. G. Yu, J. Gao, J. C. Hummelen, F. Wudi and A. J. Heeger, *Science*, 1995, **270**, 1789.
3. S. H. Park, A. Roy, S. Beaupre, S. Cho, N. Coates, J. S. Moon, D. Moses, M. Leclerc, K. Lee and Alan J. Heeger, *Nat. Photon.*, 2009, **3**, 297.
4. J. Peet, J. Y. Kim, N. E. Coates, W. L. Ma, D. Moses, A. J. Heeger and G. C. Bazan, *Nat. Mater.*, 2007, **6**, 497.
5. J.A. Hauch, P. Schilinsky, S.A. Choulis, R. Childers, M. Biele and C.J. Brabec, *Sol. Energy Mater. Sol. Cells*, 2008, **92**, 727.
6. C.H. Peters, I.T. Sachs-Quitana, J.P. Kastrop, S. Beaupré, M. Leclerc and M.D. McGehee, *Adv. Energy Mater.*, 2011, **1**, 491.
7. L-M. Chen, Z. Hong, G. Li and Y. Yang, *Adv. Mater.*, 2009, **21**, 1434.
8. C-H. Hsieh, Y-J. Cheng, P-J Li, C-H. Chen, M. Dubosc, R-M. Liang and C-S. Hsu, *J. Am. Chem. Soc.*, 2010, **132**, 4887.
9. T. Kuwabara, H. Sugiyama, M. Kuzuba, T. Yamaguchi and K. Takahashi, *Org. Elec.*, 2010, **11**, 1136.
10. H. Schmidt, K. Zilberberg, S. Schmale, H. Flugge, T. Riedl and W. Kowalsky, *Appl. Phys. Lett.*, 2010, **96**, 243305.
11. Y. Sun, J. H. Seo, C. J. Takacs, J. Seifter and A. J. Heeger, *Adv. Mater.*, 2011, **23**, 1679.
12. X. Bulliard, S. Ihn, S. Yun, Y. Kim, D. Choi, J. Choi, M. Kim, M. Sim, J. Park, W. Choi and K. Cho, *Adv. Funct. Mater.*, 2010, **20**, 4381.
13. K. S. Kim, H. Song, S. H. Nam, S.-M. Kim, H. Jeong, W. B. Kim and G. Y. Jung, *Adv. Mater.*, 2012, **24**, 792.
14. J. Hensei, G. Wang, Y. Li and J. Z. Zhang, *Nano Lett.*, 2010, **10**, 478.
15. L. G. Devi and R. Kavitha, *RSC Adv.*, 2014, **4**, 28265.
16. M. Dürr, S. Rosselli, A. Yasuda and G. Nelles, *J. Phys. Chem. B*, 2006, **110**, 21899.
17. P. S. Archana, A. Gupta, M. M. Yusoff and R. Jose, *Appl. Phys. Lett.*, 2014, **105**, 153901.
18. W. U. Huynh, J. J. Dittmer and A. P. Alivisatos, *Science*, 2002, **295**, 2425.
19. Y. S. Zhao, H. Fu, A. Peng, Y. Ma, Q. Liao and J. Yao, *Acc. Chem. Res.*, 2010, **43**, 409.
20. V. V. Kislyuk and O. P. Dimitriev, *J. Nanosci. Nanotechnol.*, 2008, **8**, 131.
21. J.-M. Zhu and H.-Y. Chen, *Adv. Mater.*, 2003, **15**, 156.
22. Y. Hu, J. Chen, W. Chen and J. Ning, *Mater. Lett.*, 2004, **58**, 2911.
23. Q. Zhang, C. S. Dandeneau, X. Zhou and G. Cao, *Adv. Mater.*, 2009, **21**, 1.
24. A. B. F. Martinson, J. W. Elam, J. T. Hupp and M. J. Pellin, *Nano Lett.*, 2007, **7**, 2183.
25. M. Yu, Y.-Z. Long, B. Sun and Z. Fan, *Nanoscale*, 2012, **4**, 2783.
26. Z. L. Wang, *Adv. Mater.*, 2003, **15**, 432.
27. I. Hod, M. Shalom, Z. Tachan, S. Rühle and A. Zaban, *J. Phys. Chem. C*, 2010, **114**, 10015.
28. J Zhang, J. H. Bang, C. Tang and P. V. Kamat, *ACS Nano*, 2010, **4**, 387.
29. H-S. Shim, S-I. Na, S. H. Nam, H-J. Ahn, H. J. Kim, D-Y. Kim and W. B. Kim, *Appl. Phys. Lett.*, 2008, **92**, 183107.
30. H. -S. Shim, J. W. Kim, Y. E. Sung and W. B. Kim, *Sol. Energy Mater. Sol. Cells*, 2009, **93**, 2062.
31. Y. S. Kim, B-K. Yu, D-Y. Kim and W. B. Kim, *Sol. Energy Mater. Sol. Cells*, 2011, **95**, 2874.
32. Y. Xia, P. Yang, Y. Sun, Y. Wu, B. Mayers, B. Gates, Y. Yin, F. Kim and H. Yan, *Adv. Mater.*, 2003, **15**, 353.
33. Z. Liang, Q. Zhang, O. Wiranwetchayan, J. Xi, Z. Yang, K. Park, C. Li and G. Cao, *Adv. Funct. Mater.*, 2012, **22**, 2194.
34. S. H. Park, A. Roy, S. Beaupré, S. Cho, N. Coates, J. S. Moon, D. Moses, M. Leclerc, K.-H. Lee and A. J. Heeger, *Nat. Photonics*, 2009, **3**, 297.
35. Y.-H. Chen, K.-C. Huang, J.-G. Chen, R. Vittal and K.-C. Ho, *Electrochim. Acta*, 2011, **56**, 7999.
36. L.-Y. Lin, M.-H. Yeh, K.-W. Tsai, C.-Y. Chen, C.-G. Wu and K.-C. Ho, *Electrochem. Commun.*, 2013, **37**, 71.